Lipid packing variations induced by pH in cardiolipin-containing bilayers: The driving force for the cristae-like shape instability

Nada Khalifat, Jean-Baptiste Fournier, Miglena Angelova, Nicolas Puff

Title:

Lipid Packing Variations Induced by pH in Cardiolipin-containing Bilayers: the Driving Force for the Cristae-like Shape Instability

Authors:

Nada Khalifat [†], Jean-Baptiste Fournier[&], Miglena I. Angelova [#&] and Nicolas Puff [# & *]

Author affiliations:

[†] UPMC Univ. Paris 06, UMR S 938, CDR St-Antoine, F-75005, Paris, France

[#] UPMC Univ. Paris 06, UFR 925, F-75005, Paris, France

[&] Laboratoire Matière et Systèmes Complexes (MSC), UMR 7057 CNRS and Université Paris Diderot - Paris 7, CC 7056, 75205 Paris, France

** Corresponding author:*

Nicolas PUFF, Ph.D
Laboratoire Matière et Systèmes Complexes (MSC), CNRS UMR 7057
Université Paris Diderot - Paris 7
Bât. Condorcet, case 7056
10, rue Alice Domon et Léonie Duquet
75205 Paris Cedex 13, France
Tél : +33 (0)1 57 27 70 82
Fax : +33 (0)1 57 27 62 11
e-mail : nicolas.puff@univ-paris-diderot.fr

Abstract
Cardiolipin is a four-tailed acidic lipid found predominantly within the inner membrane of mitochondria, and is thought to be a key component in determining inner membrane properties and potential. Thus, cardiolipin may be involved in the dynamics of the inner membrane characteristic invaginations (named cristae) that protrude into the matrix space. In previous studies, we showed the possibility to induce, by localized proton flow, a macroscopic cristae-like shape remodeling of an only-lipid model membrane mimicking the inner mitochondrial membrane. In addition, we reported a theoretical model describing the dynamics of a chemically driven membrane shape instability caused by a modification of the plane-shape equilibrium density of the lipids in the membrane. In the present work, we focus on the lipid-packing modifications observed in a model cardiolipin-containing lipid membrane submitted to pH decrease because this is the driving force of the instability. Laurdan fluorescence and ζ-potential measurements show that under pH decrease, membrane surface charge decreases, but that significant modification of the lipid packing is observed only for CL-containing membranes. Our giant unilamellar vesicle experiments also indicate that cristae-like morphologies are only observed for CL-containing lipid membranes. Taken together, these results highlight the fact that only a strong modulation of the lipid packing of the exposed monolayer leads to membrane shape instability and suggest that mitochondrial lipids, in particular the cardiolipin, play a specific role under pH modulation in inner mitochondrial membrane morphology and dynamics.

Keywords
Cardiolipin, pH, Laurdan, Mitochondria, GUV, Curvature instability

Abbreviations
CL, cardiolipin (diphosphatidylglycerol); IMM, inner mitochondrial membrane; PC, egg yolk L-α-phosphatidylcholine; PE, egg yolk L-α-phosphatidylethanolamine, LUV, large unilamellar vesicles; GUV, giant unilamellar vesicles; GP, generalized polarization; Laurdan, 6-dodecanoyl-2-dimethylaminonaphthalene; DPH, 1,6-diphenyl-1,3,5-hexatriene

1. Introduction

Cardiolipin (CL) is a divalent anionic lipid with four acyl chains. This unusual structure results from its dimeric nature, where two phosphatidyl moieties are linked together through a central glycerol group (for review see Haines [1] and Lewis et al. [2]). The structure of CL is characterised by a large hydrophobic region and a strongly charged relatively small head group, which together imply that CL favour negative curvature [3, 4] in particular if the charge in the headgroup is reduced [5, 6]. Potentially, the two phosphate groups of CL which have very different pK_a values (pK_1 < 4.0 and pK_2 > 7 [2, 7]) can carry negative charges. Ionization levels of the headgroup of CL has been found to be not only dependent of the pH but also affected by the environmental factors such as its concentration in the bilayer [8].

In biological membranes, CL is found only in the inner bacterial and mitochondrial membranes with molar concentration ranging from 5 to 20%. In the mitochondrion, CL is involved in an exceptionally broad variety of functions, including structural stabilisation of membrane proteins and respiratory complexes. Indeed, CL has high binding affinity for each of the membrane proteins that is involved in the synthesis of ATP in the mitochondrion [9-12]. Due to their charge nature, CLs are also involved in maintaining the electrochemical proton gradient across the inner mitochondrial membrane (IMM) (the matrix mean bulk pH proved to be around 8 whereas in the intermembrane space, the mean pH was estimated to be around 7.4 [13]) which enables ATP synthesis and ADP-ATP translocation [14]. Cardiolipin's intimacy with the F_0-F_1 ATP synthase together with its high headgroup pK suggests it serves as a proton source for protons used in proton-pumping during ATP synthesis [14].

The inner mitochondrial membrane is an example of a highly folded and dynamic biological structure [15, 16]. The IMM is composed of two subdomains: the inner boundary membrane (IBM) and the cristae membrane (CM). CMs are invaginations of the IMM that protrude into the matrix space. It was recently shown that topology and dynamics of the IMM are strongly linked to mitochondrial functions [17-19] but surprisingly, the components responsible for that are still largely unknown. Thus, understanding how the shape of the inner membrane is regulated on a molecular basis is of great relevance and may lead to a better understanding of mitochondrial function in general. Most of recent works focused on the role of proteins, in particular on those that induce membrane curvature by their conic-like shape as the ATP synthase dimers [20-22]. However, it remains still unclear whether the inner membrane topology and dynamics are dependent on specific mitochondrial proteins only, or/and on lipid mediated processes. Indeed, it was shown that reduced levels of CL produce aberrant cristae morphology [23] and that in a mitochondrial disorder that affects CL (Barth Syndrome), IMM presents reduced cristae density [24]. These studies clearly established a link between mitochondrial function and cardiolipin levels. Consequently, regarding the inner membrane topology and dynamics, the role of lipids and in particular of CL, has to be studied precisely in order to obtain a detailed molecular understanding of this system.

Relatively few studies of CL membranes, and of membranes composed of mixtures of CL with other lipids, have been performed. Nevertheless, some numerical [25-27] and experimental [8, 28-31] studies investigate CL effects on the structure and properties of lipid bilayers. For example, the behavior of lipid monolayers composed of binary mixtures of bovine cardiac CL and PC at the air/water interface of a Langmuir trough has been examined [30]. This study indicates that CL and PC are fully miscible with each other at all proportions tested and that CL has a condensing effect on PC monolayers. Very similar results were later presented in another monolayer film study of mixtures of bovine cardiac CL with POPC or POPE, although these works claimed to detect the existence of CL-rich and DOPE-rich domains in supported monolayer formed on a mica substrate [29]. Recently, attempts have been made to model the effect of CL on different matrices (PC, PE, and mixed PC-PE for reference [27]) using both coarse-grained [26] and atomistic molecular dynamics simulations

[27]. These studies suggest that the incorporation of CL into PC bilayers should have a significant ordering effect, predictions supported by the experimental observations described above. On the other side, Róg et al. [27] showed that the effects of CL in ternary membrane systems are complex and cannot be easily deduced from the corresponding ones in binary membranes and in particular that the surface area remains unaffected when CL is added to a mixed PC-PE bilayer membrane. To the best of our knowledge, there is only one experimental study of the mechanical properties of bilayers containing CL [30]. These authors have shown that both apparent area compressibility modulus and lysis tension decrease with increasing CL content in SOPC bilayers. These findings indicate that a lower stress is required to achieve a given change in membrane area and suggest that less energy is required to create folds in the IMM, aiding in their formation. Anyway, there is a real lack in the literature of data concerning the structure and dynamics of ternary lipid systems mimicking the IMM and, almost nothing on their behavior under pH modifications (it was yet suggested that the local pH in the intracristal compartments might be much lower than 7.4 [32, 33]). So, regarding the mitochondrion, and in particular the transmembrane pH difference between the mitochondrial matrix and the intermembrane space, it appears fundamental now to examine how the bilayer charge reduction affects the structure and the dynamics of IMM-like membranes.

In a previous study [34], we offered some original insights into the factors that determine the dynamical tubular structures of IMM cristae. We showed that the creation of a localized pH gradient induced "cristae-like" morphology in an only-lipid minimal model system (CL-containing giant unilamellar vesicles). Delivering protons onto CL-containing membranes (decreasing local pH) lead to partial charge neutralization and to area reduction of the exposed monolayer. So, the induced-area mismatch between the two monolayers of the membrane will create a mechanical stress and induce the tubular membrane invaginations. In order to have a better understanding of this chemically driven membrane shape instability, we described this phenomenon theoretically in details for the case of increasing local pH [35, 36] but this model is valid as well in the case of local acidification. We have shown that the chemical modification of the lipids of the exposed monolayer could result in a change of the spontaneous curvature and in a change of the plane-shape equilibrium density. Both of these effects have been taken into account and compared [35]. In our description of the dynamics of the instability, the intermonolayer friction plays a crucial part: it gives the longest timescale of the instability, as the monolayers are unable to slide with respect to each other on short timescales. The fact that we observed a relaxation dynamics which is well described by a mechanism involving the intermonolayer friction indicates that the change of the plane-shape equilibrium density of the exposed monolayer is important in our curvature instability.

The main purpose of this work is precisely to evaluate the effects of pH on the properties of CL- containing membranes and in particular to investigate in details lipid packing modifications, the driving force of the described-curvature instability. The degree of lipid packing can be determined with fluorescent membrane probes such as 6-dodecanoyl-2 dimethylaminonaphthalene (Laurdan) [37-40]. We analyse the modifications of the generalized polarization (GP) of CL-containing large unilamellar vesicles (LUV) exposed to different pH environments and we find that the lower the pH is, the more ordered the bilayer is. These measurements are complemented by determining the ζ-potential of the bilayers in different environments showing that membrane exposure to ions, such as protons and hydroxide ions, altered surface charge density. An additional outcome of this work is the investigation of the relationship between structural properties of membranes and giant vesicle membrane morphology. Experiments, in which giant unilamellar vesicles (GUV) were exposed to a localized pulse of acid, have been done and showed that cristae-like morphologies are induced only in CL-containing membranes. Taken together, the data support the view that lipid packing modification induced by a pH local decrease is the driving force of

the membrane shape instability and also suggest the underlying role of mitochondrial lipids, especially that of cardiolipin.

2. Materials and Methods

2.1. Chemicals

The following lipids were obtained and used without further purification: egg yolk L-α-phosphatidylcholine (PC), Sigma-Aldrich, Lyon, Rhône, France; egg L-α-phosphatidylethanolamine (PE), Avanti Polar Lipids, Alabaster, AL; heart bovine 1,3-bis(sn-3-phosphatidyl)-sn-glycerol diphosphatidylglycerol (cardiolipin, CL), Avanti Polar Lipids, Alabaster, AL. Fluorescent probes 6-dodecanoyl-2-dimethylaminonaphthalene (Laurdan), and, 1,6-diphenyl-1,3,5-hexatriene (DPH) were from Molecular Probes Inc., Eugene, OR. All others chemicals were of highest purity grade: HEPES (Interchim, Montluçon, Allier, France); EDTA (Sigma-Aldrich, Lyon, Rhône, France).

2.2. Large Unilamellar Vesicles Preparation

Large unilamellar vesicles (LUVs) were prepared using the extrusion method [41]. Samples were prepared by dissolving and mixing the indicated lipids in chloroform/methanol (9.4:0.6 v/v) to obtain the desired compositions. Thereafter the solvent was removed under a stream of oxygen-free dry nitrogen (20 min). The residues were subsequently maintained under vacuum for 2 hours and then HEPES buffer, pH 8 or 4 respectively (HEPES 5 mM, EDTA 0.1 mM) was added at room temperature (22°C) to yield a lipid concentration of 2 mM. The samples were heated at 30°C for 30 minutes, vortexed for 2 min and left in a sonication bath for 30 min, vortexed again for 1 min to ensure more uniform vesicle dispersion, and incubated again at 30°C for 15 min. The multilamellar vesicles obtained at this stage were then extruded with a LiposoFast small-volume extruder equipped with polycarbonate filters (Avestin, Ottawa, Canada) as follows: 12 extrusions through 800 nm, followed by 21 extrusions through 100 nm filters. The fluorescent probes (Laurdan and DPH) were mixed with the lipids in the initial organic solution and were used at low concentrations in order not to perturb the lipid bilayer structure (Laurdan:lipid ratio of 1:200 and DPH:lipid ratio of 1:500). LUVs samples were kept at 4°C, and used for measurements the day after.

2.3. Fluorescence Measurements

Steady-state fluorescence measurements were carried out with a Cary Eclipse spectrofluorimeter (Varian Instruments, CA) equipped with polarizers and a thermostated cuvette holder (± 0.1°C). Excitation and emission slits were adjusted to 5 nm. Fluorescence emission spectra were all recorded at 25 °C. All fluorescence measurements were carried out at a total lipid concentration of 0.2 mM.

Measurements of Laurdan generalized polarization (GP)

Laurdan is a fluorescent molecule that detects changes in membrane phase properties through its sensitivity to water molecules presented in the environment in the bilayer. Excitation wavelength for Laurdan was 355 nm. All emission spectra (from 370 to 600 nm) were recorded twice, averaged, and background subtracted. Polarity changes are shown by shifts in the Laurdan emission spectrum, which are quantified by calculating the generalized polarization (GP) defined as $GP = (I_{440} - I_{500})/(I_{440} + I_{500})$ where I_{440} and I_{500} are the emission intensities at 440 and 500 nm respectively. GP values can theoretically assume values from +1 (being most ordered) and -1 (being least ordered). GP measurements are done

by simply registering the two mentioned emission intensities (2 sets of 5 measurements averaged).

Measurements of DPH anisotropy (r_{DPH})
The membrane hydrocarbon region fluidity was measured using the fluorescent probe DPH. In fact, steady-state DPH anisotropy r_{DPH} within the bilayer, which is inversely proportional to membrane fluidity, was determined (excitation 358 nm; emission 428 nm; slit width 5 nm) using the expression $r_{DPH} = (I_{VV} - GI_{VH})/(I_{VV} + 2GI_{VH})$ where I represents the fluorescence emission intensity, V and H represent the vertical and horizontal orientation of the excitation and emission polarizers, and $G = I_{HV}/I_{HH}$ accounts for the sensitivity of the instrument towards vertically and horizontally polarized light.

2.4. ζ-potential

The ζ-potential, represents the potential slightly above the membrane interface and is related to the membrane surface charge density, was calculated from the electrophoretic mobility based on the Helmholtz–Smoluchowski relationship [42] from LUV suspensions (0.2 mM total lipid) using Nano–ZS (Red badge) ZEN 3600 (Malvern Instruments Ltd, Malvern, UK). The ζ-potential values of the vesicles were determined at pH 8 and 4.0, at 25.0 ± 0.1 °C.

2.5. Giant Unilamellar Vesicles Preparation

GUVs were formed by the liposome electroformation method [43, 44] in a thermostated chamber. The particular electroformation protocol established in this work was as follows: single lipids as well as lipid mixture solutions were prepared in chloroform/diethyl ether/methanol (2:7:1 v/v) at 1 mg/ml of total lipid. A droplet of lipid solution (1 µl) was deposited (avoiding sliding) on each of the two parallel platinum wires (diameter 0.8 mm, distance between axes 3 mm) and dried under vacuum for 15 min. An AC electrical field, 10 Hz, 0.26 V pp, was applied to the electrodes. Buffer solution (2 ml, pH 8, HEPES 0.5 mM, EDTA 0.5 mM, and temperature ~ 25°C) was added (avoiding agitation) to the working chamber. The voltage was gradually increased (over 2 h) up to 1 V pp and kept for 15 more minutes before switching the AC field off. The GUVs were ready for further utilization. In each preparation at least 10 GUVs of diameter 50 - 80 µm were available.

2.6. Imaging GUVs and Micromanipulation

We used a Zeiss Axiovert 200M microscope, equipped with a charge-coupled device camera (CoolSNAP HQ, Photometrics, Tucson, AZ, USA). The experiments were computer controlled using Metamorph software (Molecular Devices, Downington, PA, USA). The morphological transformations and the dynamics of the membrane were followed by phase contrast microscopy.

Tapered micropipettes for the local injection of HCl were made from GDC-1 borosilicate capillaries (Narishige, Tokyo, Japan), pulled on a PC-10 pipette puller (Narishige). The inner diameter of the microcapillary used for performing the local injections onto a GUV was 0. 3 µm. For these local injections, a microinjection system (Eppendorf femtojet) was used. The micropipettes were filled with an acid solution of HCl (100 mM, pH 1.6). The injected volumes were of the order of picoliters, the injection lasted a few seconds, and the injection pressure was 15-25 hPa. The positioning of the micropipettes was controlled by a high-graduation micromanipulator (MWO-202, Narishige) and the initial distance from the GUV membrane was ~10 µm taking care to avoid any contact with the lipid membrane. The hydrodynamics of the solution injected by the micropipette could be visualized and thereby we could evaluate that the part of the GUV membrane directly affected by the microinjection

was about 10%. Visualizing the flux from the micropipette allows estimating as well the dilution of acid solution after injection. We calibrated the pH in function of the dilution of 100 mM HCl pH 1.6 in the buffer in which the GUV were formed. That allows us to estimate the local pH value effectively created at the GUV membrane during the HCl delivery to be about pH 4 to 5 [34].

3. Results and discussion

3.1. Properties of model membrane mimicking IMM under pH modifications

PC, PE and CL represent the most abundant phospholipid components of the inner mitochondrial membrane (IMM) and thus are used as constituents for IMM mimetic systems [45-47]. Therefore, we made our vesicular mimetic systems from PC/PE/CL 60:30:10 mol/mol. In order to study the effect of pH on the hydration and viscosity of the lipid bilayer, we included some fluorescent probes (Laurdan, DPH) in LUV lipid membranes. These fluorescent molecules localize at different depths in the lipid bilayer, thereby yielding information on the lipid membrane's global properties.

The wavelength of the Laurdan emission peak is dependent of the presence of water in the membrane. Because water penetration into the bilayer is directly related to inter-lipid spacing, Laurdan has been used to measure the degree of lipid packing [37, 38]. We present in Fig. 1a Laurdan fluorescence spectra recorded at different pH values of LUV suspension medium ranging from 8.01 to 2.46. In these experiments, we gradually lowered the pH of the LUV sample by adding aliquots of acid solution (10 or 100 mM HCl). After few minutes equilibration under agitation, the spectra were recorded assuming that the system has reached a steady-state. Indeed, it was demonstrated that only few hundreds of seconds after aliquot addition are necessary to equilibrate the internal leaflet to the new pH [48, 49]. As pH values decrease, there is a decrease of the mean intensity of the spectrum combined with a shift of the spectral maximum to shorter wavelength. Data show that upon decreasing of pH of the external medium the peak at 440 nm becomes more pronounced, i.e., the GP value increases at low pH. Indeed, as explained in the Materials and Methods, the effects of pH on the spectra could be quantified by calculation of the generalized polarization (GP) for each emission spectrum. As shown in Fig. 1b, the values of Laurdan GP increase with decreasing pH values of the bulk phase. For example, the Laurdan GP rise from -0.012 (pH 8.01) to +0.220 (pH 2.46). Fig. 1c and 1d depict spectra and GP values calculated from the Laurdan emission spectra for control experiments. In these experiments, instead of HCl, we injected buffer solution only to check for any eventual dilution effect. We observed that under dilution, there is no shift of the spectral maximum of the spectra (Fig. 1c) and thus, GP values remain the same whatever the dilution (Fig. 1d). Fig. 1e shows both the Laurdan GP (○) and the anisotropy of DPH (■) variations during progressive acidification of the LUV suspension medium. Here, GP values were calculated for eleven pH values ranging from 2.46 to 8.01, while r_{DPH} values were calculated for eight pH values ranging from 3.00 to 8.01.This figure illustrates more precisely than in Fig. 1b the Laurdan GP shift to higher values observed upon successive proton additions in the bulk phase and the capability of Laurdan to sense progressively tighter lipid packing. As we can see in Fig. 1e, between pH 5.5 and 8.0, GP values remain more or less constant while below pH 5.5, GP values increase especially as the pH is low. This increase of the GP values in acidic medium reflects the progressive dehydration and increasing apolarity (structuring) close to the water/lipid interface. Fig. 1e also depicts the anisotropy of DPH, giving information about membrane hydrophobic core fluidity. We observe that there is no r_{DPH} significant variation under the entire pH range

studied and therefore, the membrane fluidity does not change despite the acidification of the medium.

Our experiments involving Laurdan fluorescence reveal that the progressive dehydration of the bilayer under pH decrease causes a more efficient lipid packing, as water penetration into the bilayer is directly related to inter-lipid spacing. The decrease in the mean area per headgroup with decreasing pH can be easily understood by considering in particular the number of charge molecules in the system. When the fraction of protonated or partially protonated CL increases with decreasing pH, the repulsive interaction between CL headgroups decreases. Changing CL charge reduces electrostatic repulsion and increases hydrogen bonding which together lowers the effective size of the headgroup. Concerning the zwitterionic lipids in the membrane (PC and PE), none of their functional groups has a pK_a within the range of pH 2.5 to 8 [50]. pH effect most likely results from other physical interactions, such as counterion binding and partitioning into the membrane [51]. Zwitterionic PC and PE molecules contain functional groups, whose electric charge distribution at the membrane interface is a function of the binding of counterions like protons and hydroxide ions. Anyway, both of these mechanisms act in reducing the negative surface charge. This latter point is confirmed by our ζ-potential measurements (Table 1) indicating that a decrease of the pH suspension medium from 8 to 4 corresponds respectively to a change of the ζ-potential from -56 mV to -46.4 mV for the model membrane mimicking the IMM. We conclude that the pH affects both the surface charge and the mean area per molecule and that the resulting changes in the electrostatic environment influence strongly the very structure of the model membrane mimicking IMM.

3.2. Fundamental role of CL in membrane properties under proton addition

We carried out the same kind of Laurdan GP measurements (Fig. 2a) and ζ-potential measurements (Table 1) on one hand with LUVs containing only PC and CL (PC/CL 90:10 mol/mol), and on the other hand, with LUVs that do not contain CL (made only of PC, or PC/PE 66:34 mol/mol). Our purpose here was to investigate the relative part of each membrane lipid component on the membrane behaviour under pH modifications.

Fig. 2a shows for different kind of bilayers the GP evolution during a progressive acidification of the LUV suspension medium. First, we can notice that at pH 8 (and it's still true at physiological pH), the calculated values of GP are strongly different for the bilayers that contain or not PE. The PC bilayers are the more hydrated membranes (therefore, the less-packed), followed by the bilayer composed of a mixture of PC and CL solely. As we can see in Fig. 2a, the presence of PE induces an important increase of the GP value whether or not CL presence. So, for the lipid systems tested, PE tends to make more ordered bilayers. It's important to highlight here that, at pH close to the physiological one, the addition of CL to a binary system made of PC and PE doesn't change the calculated GP value. Secondly, for CL-containing membranes (□: PC/CL 90:10 mol/mol and ○: PC/PE/CL 60:30:10 mol/mol) under progressive acidification, the GP remains stable down to pH 5.5 and then begins to increase strongly. On the contrary, for bilayers without CL (●: PC and ▲: PC/PE 66:34 mol/mol), GP remains stable down to a lower pH value (about pH 4). There is nevertheless a small increase in the GP for lower pH values than 4. So, whatever the bilayer composition, a strong decrease of pH leads to a GP shift to higher values, but this rise of GP is only significant for CL-containing membranes. As we do for model membrane mimicking IMM, we measured for all the systems studied the ζ-potential at pH 4 and pH 8. Table 1 summarizes and compares these values.

The analysis of our experiments underlines the fact that the lipid composition plays a major role in determining the bilayer lateral structure, and in particular, under pH variation. The analysis of the different GP values at physiological pH allows us to confirm some results

already obtained by others groups either experimentally or numerically. Indeed, our Laurdan fluorescence experiments show that the addition of 10 % mol CL to PC bilayers (Fig. 2a, ● and □ at pH 7.4) leads to a bilayer condensation. This effect was already highlighted by thermodynamic analysis of monolayer compression isotherms [29, 30] or by dynamics simulations [25, 27]. We also notice that the addition of 10 mol % CL to a mixed PC/PE bilayer membrane doesn't have any influence on the calculated GP at physiological pH (Fig. 2a, ○ and ▲ at pH 7.4). This result is consistent with atomic-scale molecular dynamics simulations [27] and shows that in presence of PE, CL addition doesn't lead to membrane condensation. Secondly, the analysis of the curves presented in Fig. 2a shows that only membranes containing a lipid with titratable groups (CL) present a significant rise of the GP values. For these membranes, the variation of the GP values between pH 2.46 and pH 8.01 is about 0.25, variation consistent with the measurement done for the binary system PC/CL in [38]. In the case of binary systems without CL (Fig. 2a, ● and ▲), the small better packing observed at very low pH corresponds to counterions binding. This idea and our results are in agreement with Langmuir monolayer experiments in which the area per molecule of PE monolayer decreased when the pH was decreased from pH 7 to pH 3 [52]. For monolayer of PC only, Fujiwara et al. [53] found that no significant differences were observed among the isotherms of monolayers formed at pH 7.0 and 3.5, but this is consistent with the fact that in our experiments, GP really increases below pH 3. So, it appears now clear that there is only a significantly increased bilayer packing in presence of CL. In order to compare easily the variations of the GP values, we calculate separately for each different lipid system the difference ΔGP between the GP value and its initial value at pH 8. Fig. 2b plots the ΔGP variations during the progressive acidification of the LUV suspension medium. One can notice that the ΔGP variations are practically the same for CL-containing membranes with and without PE (Fig. 2b, ○ and □). So, concerning the lipid packing modification under acidification, PE doesn't seem to have any influence. Taken together, Laurdan fluorescence and ζ-potential data show that whatever the bilayer under pH decrease, absolute surface charge decreases but a significant modification of the lipid packing takes place only for CL-containing membranes.

3.3. Tubular shape invagination of GUV membrane under local pH modulation

In these experiments, our goal was to mimic as simply as possible the dynamic morphology of the inner mitochondrial membrane. The IMM was modelled by the membrane of a GUV formed at pH 8, and the proton concentration difference observed *in vivo* between the matrix and the intermembrane space was mimicked by local addition (by a micropipette) of an acidic solution. Indeed, pH was locally modulated in real time (lowered and then let to rise to the initial bulk value) as a result of the delivering (or not) of HCl solution (100 mM) at the outer side of the GUV membrane. The microinjection parameters were the same for the vesicles shown in Figs. 3-5 (inner micropipette diameter, 0.3 µm; injection pressure 15-25 hPa). The GUV composition mimicking the IMM was PC/PE/CL 60:30:10 mol/mol, but, in order to highlight the particular role of CL, we also carried out experiments with GUVs made from lipid binary compositions used in our Laurdan fluorescence measurements. One can see in Fig. 3 (PC/PE/CL 60:30:10 mol/mol) the initial GUV (Fig. 3, frame 0 s), the micropipette near the vesicle membrane (Fig. 3, frame 9.9 s), the induced invagination (Fig. 3, frame 27.6 s), and the development of characteristic morphology (Fig. 3, frames 28.5 s to 42 s). In a first work [34], we identified this morphology as "cristae-like" because it mimics very well the IMM morphology shown by 3D electron microscopy. As soon as the acid delivery is off, the membrane invagination regresses and completely disappears when the local pH gradient vanishes (Fig. 3, frames 56.7 s to 87.1 s). So, this cristae-like morphology is dynamic and reversible, modulated by the local pH difference. Control experiments, and the dependence of

the GUV initial states on the invaginations shapes and typical sizes are discussed precisely in Ref. [34]. In order to study in details the role of CL in the development of such morphologies, we carried out experiments with GUV containing only PC (data not shown), PC and PE (PC/PE 66:34 mol/mol, Fig. 4), and PC and CL (PC/CL 90:10 mol/mol, Fig. 5). In the latter case (Fig. 5), the effects of local pH modulations were similar to those observed with GUV made of PC/PE/CL 60:30:10 mol/mol (development then regression of the induced invagination). On the contrary, for GUV without CL, no cristae-like morphology was observed (Fig. 4). These results indicate that CL plays a crucial role in the development of the specific cristae-like morphology in our GUV model membranes.

In the GUV experiments, the hydrodynamics of the solution injected by the micropipette could be visualized and allowed us to roughly estimate the local pH at the membrane level to be about pH 4. We assume that the inner monolayer is little affected by the pH decrease outside the vesicle because the permeation coefficient of protons through a lipid membrane is low ($P_{H+} \approx 10^{-9}$ cm/s [54]), which yields a negligible pH decrease inside the vesicle on the timescale of our GUV experiments. So, there is one monolayer of the GUV facing an acidic compartment while the other faces a neutral one. Only the lipids of the outer leaflet are then chemically modified and, as it was shown in our Laurdan fluorescence measurements if the membrane contains CL, the outer monolayer is significantly better packed. So, the outer leaflet of the CL-containing giant vesicle undergoes a condensation while the inner leaflet remains unchanged, thus creating a local elastic stress required for tubule formation. Fig. 6 summarises GP values at pH 4 and pH 8 for the different lipid systems studied. One can see in this figure that a significant modification of the lipid packing (the increase of GP corresponds to membrane condensation) is only observed for CL-containing membranes. This is consistent with the fact that, in the GUV experiments, cristae-like morphologies were only observed for CL-containing membranes. This result also consolidates our theorical description in which the change of the plane-shape equilibrium density of the exposed monolayer, in other words the lipid packing, is the driving force of the membrane shape instability. Fig. 7 proposes a qualitative description of the dynamics of the instability based on our theoretical model [36]. At $t = 0$, the *preferred* area per lipid in the external monolayer suddenly decreases in front of the pipette, due to the charge neutralization induced by the rise in pH, which lowers inter-lipid repulsion. These modified lipids are "effectively dilated", in the sense that their area per molecule is larger than their equilibrium value. In Fig.7, the preferred area per lipid is indicated on each lipid by a "constitutive sphere" the color of which indicates whether the monolayer is effectively dilated or compressed (red or dark grey) or at equilibrium (green or light grey). In Fig. 7a, corresponding to $t < 0$, the lipids have their initial equilibrium area, and so their constitutive spheres are exactly in contact (green/light grey). Conversely, at $t = 0$, i.e., just after the chemical modification (Fig. 7b), the constitutive spheres of the lipids of the outer-monolayer are no longer in contact (red/dark grey), which illustrates the fact that their density is lower than what their new equilibrium density would require. Note that we describe here the dynamics of the instability: in Fig. 7b the lipids of the outer-monolayer have been modified but have not have time to move yet. Now, one would expect the lipids of the outer-monolayer to move closer in a very short time in order to gain their new equilibrium density. However, this simple view disregards the inter-monolayer friction: as shown in [36] it takes a few seconds for the lipids of one monolayer to slide relative to those of the other monolayers for vesicles in such low-tension state as in our experiment and for such lengths scales as those corresponding to the width of the chemical modification. Hence, the dynamical picture is quite different. First, in a very short time (less than a μs), all the lipids of the affected region move in both monolayers in such a way as to increase the density (Fig. 7c). This adjustment, which relaxes about the three-quarters of the dilation energy of the outer monolayer (while creating a lesser compression energy in the inner-monolayer) is very fast; indeed, it involves

no inter-monolayer sliding of the lipids. In this stressed state (Fig.7 c), the dilation forces within the membrane tends at the same time to bend the membrane and to adjust the densities by an inter-monolayer sliding of the lipids [36]. The former mechanism turns to be the faster one, i.e., the one effectively observed just after the chemical modification (Fig. 7d). Note that curving the membrane effectively brings both monolayers in an optimum density state (green or light gray constitutive spheres). Let us now try to estimate from the above curvature-inducing mechanism how the tube grows and at which velocity. As shown in [36] the typical time scale required to curve the membrane under such dilative stresses is (apart from an unimportant logarithmic correction) of order $\tau \sim \eta\, d\, /\, (\sigma + \pi\kappa/d^2)$, where d is the length-scale of the deformation. If we consider that this is the time required to create a portion of tube of radius d, we may assume that the tubule grows where the chemical modification takes place, i.e., at its base, with a typical velocity of $v \sim d\, /\, \tau \sim (\sigma + \pi\kappa/d^2)\, /\, \eta$. Taking the example of Fig.5 between times 10.8 s and 11.1 s, we assume a very low tension $\sigma \sim 10^{-9}$ J/m^2 (floppy vesicle), a standard bending modulus $\kappa \sim 10^{-19}$ J, the viscosity of water $\eta \sim 10^{-3}$ Js/m^3, $d \sim 4$ μm for the tubule diameter, we obtain the typical velocity v ~ 20 μm/s, in agreement with a growth of order 5 μm in a lapse of 0.3 s. Note that, as better seen in Fig. 3, the tube wiggles as it grows, which is compatible with our hypothesis the tubes grows from its base. Finally, the relaxation of the tubes is very slow, as it is driven by the retro-diffusion of the H^+ ions outer of the tube. In the absence of quantitative measurements of the pH-field within and outside the tubes, it is difficult to address theoretically the dynamics of the tube retraction.

In this paper, we reported experiments in which a local curvature is observed when GUV's membrane mimicking the IMM is subjected to a local pH decrease. We showed that the chemical modification of the lipids, and in particular the protonation of cardiolipin, resulted in a change of the lipid packing, but that only a strong modification of this packing could lead to the development of cristae-like structures. This membrane behaviour is only observable when the artificial membrane mimicking the IMM contains CL, the only anionic lipid presented in our model bilayer. So, with a simple experimental model, we bring some answers suggesting that at least at the membrane level, an only-lipid system can exhibit structures closed morphologically and dynamically to those observed in the mitochondria. Our results also suggest that the main driving force for the shape transformation of the GUVs is the local change of the preferred area per lipid. Dahlberg et al. [26] provide a complementary explanation of the GUV shape transformation based on the study of the mechanical properties of coarse-grained bilayers formed by CL and zwitterionic lipids. One finding from this study is that the rigidity of the bilayer is correlated to the effective headgroup volume, so that small headgroups were associated with lower bending moduli. This is consistent with the notion that small headgroup volumes tend to give negative curvatures. They note that the inclusion of protonated-CL decreased the rigidity of the bilayer, which is compatible with highly curved membranes and therefore, for our nonequilibrium vesicle system. More precisely, we believe that the main driving force for the shape transformation of the GUVs is the local change of the preferred area per lipid, but that the decrease of the bending modulus is a promoting factor (because the energy cost for shape transformation is lower) in particular for highly curved membrane as cristae-like structure.

4. Conclusion

We investigate in this work the behavior of an artificial membrane mimicking the inner mitochondrial membrane under pH modulations in order to highlight the possible role of cardiolipin in the dynamics of mitochondrial cristae. Laurdan fluorescence and ζ-potential measurements show that, when the pH decreases and whatever the lipid composition based on the major components of the IMM, the surface charge decreases but that only CL-containing membranes exhibit a significant modification of the lipid packing. Our GUV experiments also

indicate that cristae-like morphologies were only observed for CL-containing membranes. Taken together, these results indicate on one hand the crucial role of cardiolipin in IM morphology and dynamics, and on the other hand, that the driving force of the observed shape instability might be the change of the plane-shape equilibrium density of the exposed monolayer as pointed out by our theoretical description.

Acknowledgements
We thank N. Henry for helping us in the ζ-potential measurements and M. Seigneuret for helpful discussions.

References

[1] T.H. Haines, A new look at Cardiolipin, Biochimica et biophysica acta 1788 (2009) 1997-2002.
[2] R.N. Lewis, R.N. McElhaney, The physicochemical properties of cardiolipin bilayers and cardiolipin-containing lipid membranes, Biochimica et biophysica acta 1788 (2009) 2069-2079.
[3] K.C. Huang, R. Mukhopadhyay, N.S. Wingreen, A curvature-mediated mechanism for localization of lipids to bacterial poles, PLoS computational biology 2 (2006) e151.
[4] K.E. McAuley, P.K. Fyfe, J.P. Ridge, N.W. Isaacs, R.J. Cogdell, M.R. Jones, Structural details of an interaction between cardiolipin and an integral membrane protein, Proceedings of the National Academy of Sciences of the United States of America 96 (1999) 14706-14711.
[5] M. Dahlberg, Polymorphic phase behavior of cardiolipin derivatives studied by coarse-grained molecular dynamics, The journal of physical chemistry 111 (2007) 7194-7200.
[6] R.N. Lewis, R.N. McElhaney, Surface charge markedly attenuates the nonlamellar phase-forming propensities of lipid bilayer membranes: calorimetric and (31)P-nuclear magnetic resonance studies of mixtures of cationic, anionic, and zwitterionic lipids, Biophys J 79 (2000) 1455-1464.
[7] Kates, M, S.Y.Z. Jing-Yi, Gosser, D, Haines, H. T, pH-Dissociation characteristics of cardiolipin and its 2'-deoxy analogue, LIPIDS, vol. 28, Springer, Heidelberg, 1993, p. 877.
[8] S. Nichols-Smith, T. Kuhl, Electrostatic interactions between model mitochondrial membranes, Colloids and surfaces 41 (2005) 121-127.
[9] K.S. Eble, W.B. Coleman, R.R. Hantgan, C.C. Cunningham, Tightly associated cardiolipin in the bovine heart mitochondrial ATP synthase as analyzed by 31P nuclear magnetic resonance spectroscopy, The Journal of biological chemistry 265 (1990) 19434-19440.
[10] L.I. Horvath, M. Drees, K. Beyer, M. Klingenberg, D. Marsh, Lipid-protein interactions in ADP-ATP carrier/egg phosphatidylcholine recombinants studied by spin-label ESR spectroscopy, Biochemistry 29 (1990) 10664-10669.
[11] K. Pfeiffer, V. Gohil, R.A. Stuart, C. Hunte, U. Brandt, M.L. Greenberg, H. Schägger, Cardiolipin stabilizes respiratory chain supercomplexes, J. Biol. Chem. 278 (2003) 52873- 52880.
[12] N.C. Robinson, Functional binding of cardiolipin to cytochrome c oxidase, Journal of bioenergetics and biomembranes 25 (1993) 153-163.

[13] J. Llopis, J.M. McCaffery, A. Miyawaki, M.G. Farquhar, R.Y. Tsien, Measurement of cytosolic, mitochondrial, and Golgi pH in single living cells with green fluorescent proteins, Proc. Natl. Acad. Sci. U.S.A. 95 (1998) 6803-6808.
[14] T.H. Haines, N.A. Dencher, Cardiolipin: a proton trap for oxidative phosphorylation, FEBS Lett. 528 (2002) 35-39.
[15] D.C. Logan, The mitochondrial compartment, J. Exp. Bot. 57 (2006) 1225-1243.
[16] C.A. Mannella, M. Marko, K. Buttle, Reconsidering mitochondrial structure : new views of an old organelle, Trends Biochem. Sci. 22 (1997) 37-38.
[17] T.G. Frey, C.W. Renken, G.A. Perkins, Insight into mitochondrial structure and function from electron tomography, Biochimica et biophysica acta 1555 (2002) 196-203.
[18] C.A. Mannella, The relevance of mitochondrial membrane topology to mitochondrial function, Biochim. Biophys. Acta 1762 (2006) 140-147.
[19] C.A. Mannella, Structure and dynamics of the mitochondrial inner membrane cristae, Biochim. Biophys. Acta 1763 (2006) 542-548.
[20] N.V. Dudkina, J. Heinemeyer, W. Keegstra, E.J. Boekema, H.P. Braun, Structure of dimeric ATP synthase from mitochondria: An angular association of monomers induces the strong curvature of the inner membrane, FEBS Lett. 579 (2005) 5769-5772.
[21] M.F. Giraud, P. Paumard, V. Soubannier, J. Vaillier, G. Arselin, B. Salin, J. Schaeffer, D. Brethes, J.P. di Rago, J. Velours, Is there a relationship between the supramolecular organization of the mitochondrial ATP synthase and the formation of cristae?, Biochimica et biophysica acta 1555 (2002) 174-180.
[22] M. Strauss, G. Hofhaus, R.R. Schroder, W. Kuhlbrandt, Dimer ribbons of ATP synthase shape the inner mitochondrial membrane, The EMBO journal 27 (2008) 1154-1160.
[23] E. Mileykovskaya, W. Dowhan, Cardiolipin membrane domains in prokaryotes and eukaryotes, Biochimica et biophysica acta 1788 (2009) 2084-2091.
[24] D. Acehan, Y. Xu, D.L. Stokes, M. Schlame, Comparison of lymphoblast mitochondria from normal subjects and patients with Barth syndrome using electron microscopic tomography, Lab Invest 87 (2006) 40-48.
[25] M. Dahlberg, A. Maliniak, Molecular dynamics simulations of cardiolipin bilayers, The journal of physical chemistry 112 (2008) 11655-11663.
[26] M. Dahlberg, A. Maliniak, Mechanical Properties of Coarse-Grained Bilayers Formed by Cardiolipin and Zwitterionic Lipids, Journal of Chemical Theory and Computation 6 (2010) 1638-1649.
[27] T. Rog, H. Martinez-Seara, N. Munck, M. Oresic, M. Karttunen, I. Vattulainen, Role of cardiolipins in the inner mitochondrial membrane: insight gained through atom-scale simulations, The journal of physical chemistry 113 (2009) 3413-3422.
[28] O. Domenech, L. Redondo, L. Picas, A. Morros, M.T. Montero, J. Hernandez-Borrell, Atomic force microscopy characterization of supported planar bilayers that mimic the mitochondrial inner membrane, J Mol Recognit 20 (2007) 546-553.
[29] O. Domenech, F. Sanz, M.T. Montero, J. Hernandez-Borrell, Thermodynamic and structural study of the main phospholipid components comprising the mitochondrial inner membrane, Biochimica et biophysica acta 1758 (2006) 213-221.
[30] S. Nichols-Smith, S.Y. Teh, T.L. Kuhl, Thermodynamic and mechanical properties of model mitochondrial membranes, Biochim. Biophys. Acta 1663 (2004) 82-88.
[31] S. Sennato, F. Bordi, C. Cametti, C. Coluzza, A. Desideri, S. Rufini, Evidence of domain formation in cardiolipin-glycerophospholipid mixed monolayers. A

thermodynamic and AFM study, The journal of physical chemistry 109 (2005) 15950-15957.
[32] C.A. Mannella, M. Marko, K. Buttle, Reconsidering mitochondrial structure: new views of an old organelle, Trends in Biochemical Sciences 22 (1997) 37-38.
[33] R.J.P. Williams, Mitochondria and chloroplasts: localized and delocalized bioenergetic transduction, Trends Biochem. Sci. 25 (2000) 479.
[34] N. Khalifat, N. Puff, S. Bonneau, J.-B. Fournier, M.I. Angelova, Membrane Deformation Under Local pH Gradient: Mimicking Mitochondrial Cristae Dynamics, Biophys. J. (2008) biophysj.108.136077.
[35] A.F. Bitbol, J.B. Fournier, M.I. Angelova, N. Puff, Dynamical membrane curvature instability controlled by intermonolayer friction, J. Phys.: Condens. Matter 23 (2011) 284102.
[36] J.B. Fournier, N. Khalifat, N. Puff, M.I. Angelova, Chemically triggered ejection of membrane tubules controlled by intermonolayer friction, Physical review letters 102 (2009) 018102.
[37] L.A. Bagatolli, T. Parasassi, G.D. Fidelio, E. Gratton, A model for the interaction of 6-lauroyl-2-(N,N-dimethylamino)naphthalene with lipid environments: implications for spectral properties, Photochemistry and photobiology 70 (1999) 557-564.
[38] K. Christensen, H.S. Bose, F.M. Harris, W.L. Miller, J.D. Bell, Binding of steroidogenic acute regulatory protein to synthetic membranes suggests an active molten globule, The Journal of biological chemistry 276 (2001) 17044-17051.
[39] T. Nyholm, M. Nylund, A. Soderholm, J.P. Slotte, Properties of palmitoyl phosphatidylcholine, sphingomyelin, and dihydrosphingomyelin bilayer membranes as reported by different fluorescent reporter molecules, Biophys J 84 (2003) 987-997.
[40] T. Parasassi, G. De Stasio, A. d'Ubaldo, E. Gratton, Phase fluctuation in phospholipid membranes revealed by Laurdan fluorescence, Biophys J 57 (1990) 1179-1186.
[41] R.C. MacDonald, R.I. MacDonald, B.P. Menco, K. Takeshita, N.K. Subbarao, L.R. Hu, Small-volume extrusion apparatus for preparation of large, unilamellar vesicles, Biochim. Biophys. Acta 1061 (1991) 297-303.
[42] D.E. Budil, S. Lee, S. Saxena, J.H. Freed, Nonlinear-Least-Squares Analysis of Slow-Motion EPR Spectra in One and Two Dimensions Using a Modified Levenberg-Marquardt Algorithm, Journal of Magnetic Resonance, Series A 120 (1996) 155-189.
[43] M.I. Angelova, D.S. Dimitrov, A mechanism of liposome electroformation, Prog. Colloid Polymer Sci. 76 (1988) 59-67.
[44] N. Puff, A. Lamaziere, M. Seigneuret, G. Trugnan, M.I. Angelova, HDLs induce raft domain vanishing in heterogeneous giant vesicles, Chemistry and physics of lipids 133 (2005) 195-202.
[45] A. Bruce, Skeletal muscle lipids. II. Changes in phospholipid composition in man from fetal to middle age, Journal of lipid research 15 (1974) 103-108.
[46] G. Daum, J.E. Vance, Import of lipids into mitochondria, Prog. Lipid Res. 36 (1997) 103-130.
[47] B. Gomez, Jr., N.C. Robinson, Quantitative determination of cardiolipin in mitochondrial electron transferring complexes by silicic acid high-performance liquid chromatography, Analytical biochemistry 267 (1999) 212-216.
[48] Q.-P. Chen, Q.-T. Li, Effect of Cardiolipin on Proton Permeability of Phospholipid Liposomes: The Role of Hydration at the Lipid-Water Interface, Archives of Biochemistry and Biophysics 389 (2001) 201-206.
[49] P. Soucaille, M. Prats, J.F. Tocanne, J. Teissie, Use of a fluorescein derivative of phosphatidylethanolamine as a pH probe at water/lipid interfaces, Biochimica et biophysica acta 939 (1988) 289-294.

[50] J.-F. Tocanne, J. Teissié, Ionization of phospholipids and phospholipid-supported interfacial lateral diffusion of protons in membrane model systems, Biochimica et Biophysica Acta (BBA) - Reviews on Biomembranes 1031 (1990) 111-142.
[51] Y. Zhou, R.M. Raphael, Solution pH alters mechanical and electrical properties of phosphatidylcholine membranes: relation between interfacial electrostatics, intramembrane potential, and bending elasticity, Biophys J 92 (2007) 2451-2462.
[52] N. Vila-Romeu, M. Nieto-Suárez, M. Broniatowski, The interaction of cyclodextrins with phosphatidylethanolamine Langmuir monolayers: Influence of the spreading solvent and subphase conditions, Thin Solid Films 516 (2008) 8852-8859.
[53] M. Fujiwara, R.H. Grubbs, J.D. Baldeschwieler, Characterization of pH-Dependent Poly(acrylic Acid) Complexation with Phospholipid Vesicles, J Colloid Interface Sci 185 (1997) 210-216.
[54] Y. Nozaki, C. Tanford, Proton and hydroxide ion permeability of phospholipid vesicles, Proceedings of the National Academy of Sciences 78 (1981) 4324-4328.

Figures

Fig. 1. pH dependence of GP and r_{DPH} of lipid membrane mimicking the IMM. LUV are made of PC/PE/CL 60:30:10 mol/mol with a Laurdan: lipid ratio of 1/200 or a DPH: lipid ratio of 1/500 respectively in buffer pH 8. All measurements were carried out at a lipid concentration of 0.2 mM and were recorded at 25°C. pH of the LUV samples was gradually lowered by adding aliquots of acid solution (10 or 100 mM HCl). After few minutes equilibration under agitation, the measurements were done. **(a)** Laurdan fluorescence emission spectra (λ_{exc} = 355 nm) recorded at different pH (spectrum from top to bottom at pH 8.01, 6.08, 4.41, 3.30 and 2.46). **(b)** Calculated Laurdan GP at pH values corresponding to the spectra presented in (a). **(c)** Laurdan fluorescence emission spectra recorded at different dilutions (spectrum from top to bottom at dilution factors 1, 1.033, 1.075, 1.092 and 1.15). **(d)** Calculated Laurdan GP at dilutions corresponding to the spectra presented in (c). **(e)** pH dependence of the inner mitochondrial model membrane GP (○) and r_{DPH} (■).

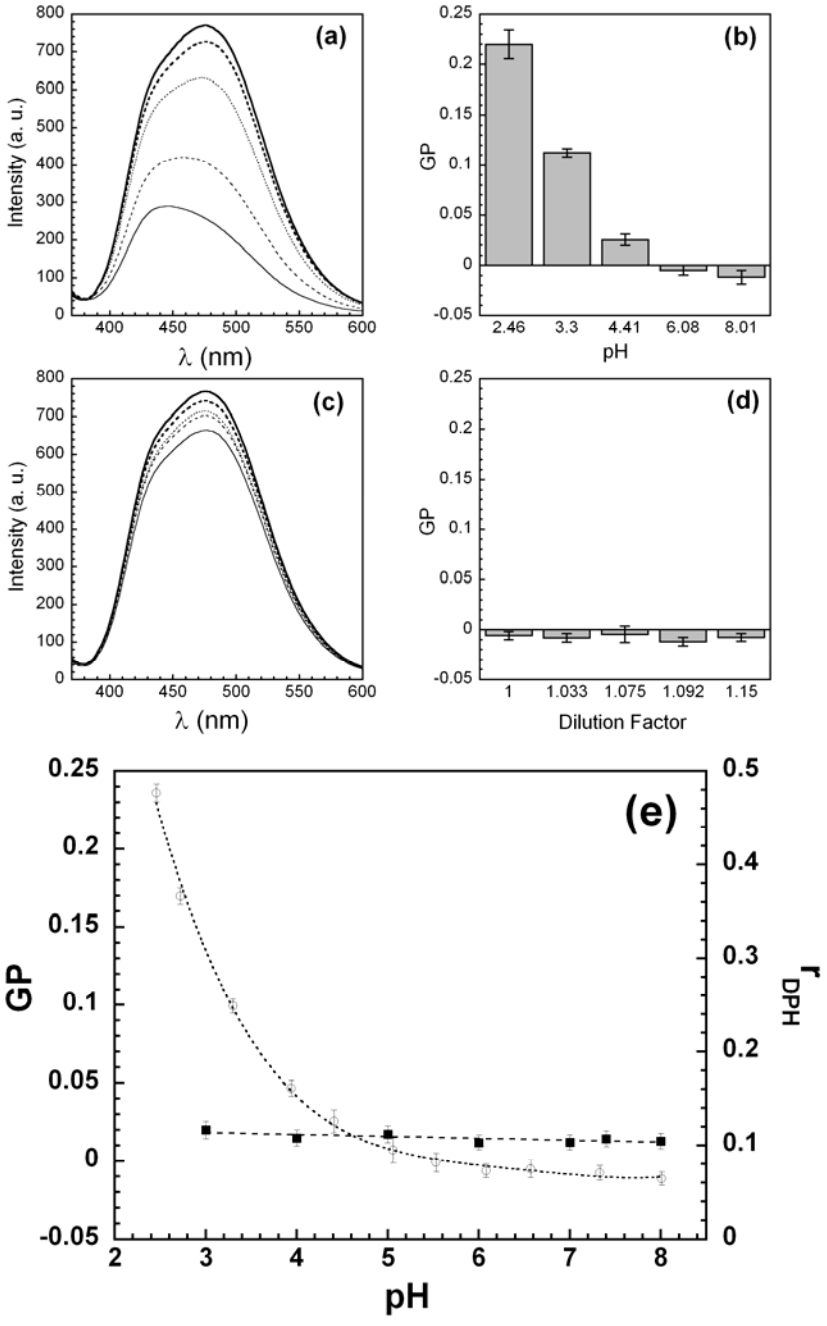

Fig. 2. Effect of the medium pH: (a) on the GP, and, (b) on the ΔGP. LUV are made of different lipid compositions with a Laurdan: lipid ratio of 1/200 in buffer pH 8. (●) PC; (□) PC/CL 90:10 mol/mol; (▲) PC/PE 66:34 mol/mol; (○) PC/PE/CL 60:30:10 mol/mol. All measurements were carried out at a lipid concentration of 0.2 mM and were recorded at 25°C. pH of the LUV samples was gradually lowered by adding aliquots of acidic solution (10 or 100 mM HCl). Measurements were made after few minutes equilibration under agitation. ΔGP is the difference between the GP value and its initial value at pH 8.

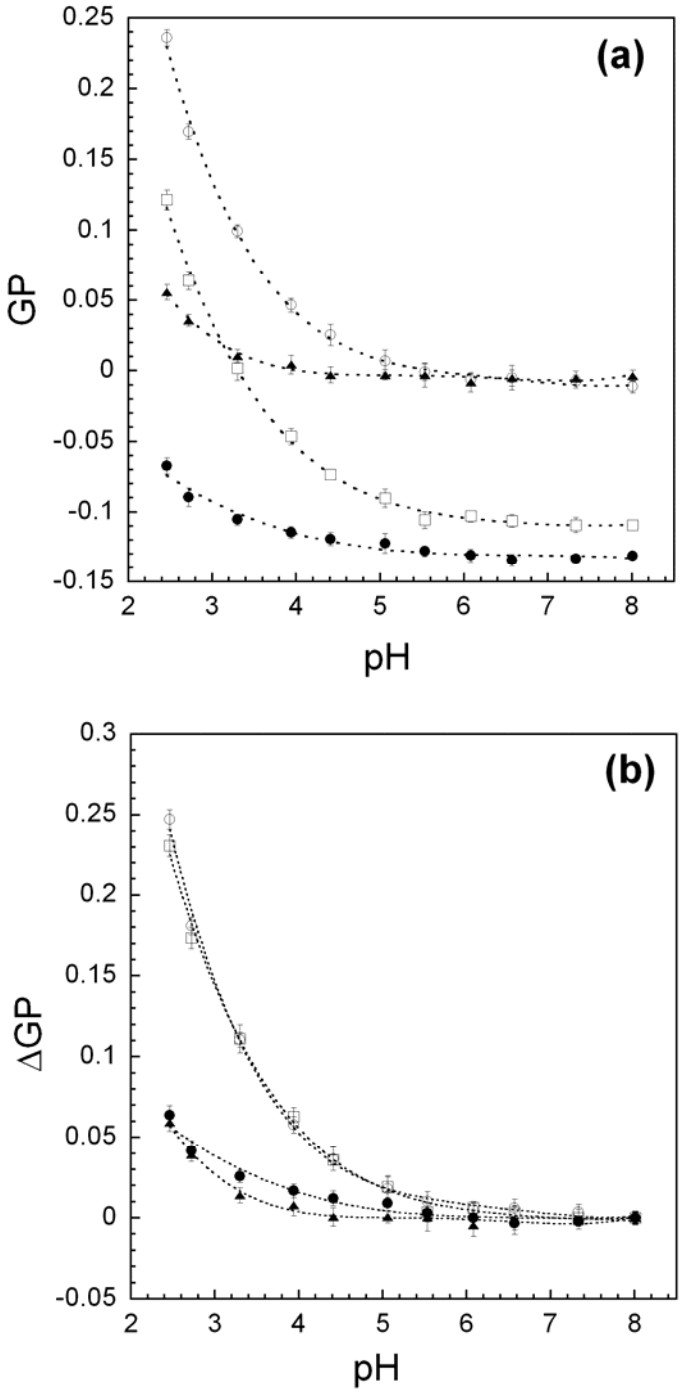

Fig. 3. Model membrane mimicking the IMM exhibiting dynamic cristae-like morphology. GUV is made of PC/PE/CL 60:30:10 mol/mol in buffer pH 8. Membrane invagination is triggered by a local pH modulation made with a micropipette delivering an acidic solution (100 mM HCl, pH 1.6). The induced membrane invagination (frame t = 42 s) is completely reversible (frames 56.7-87.1 s) as far as the acid delivery is stopped.

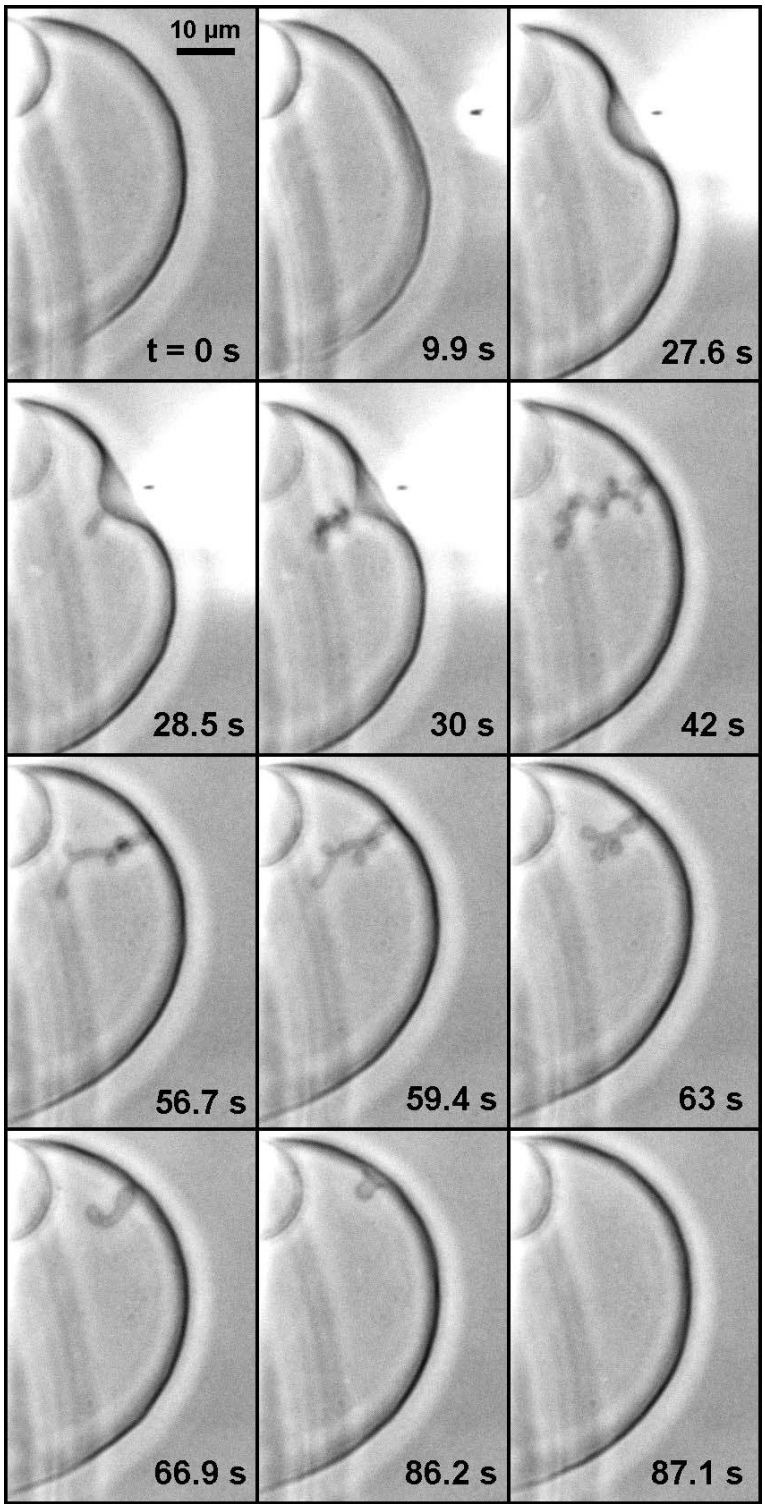

Fig. 4. Crucial role of CL in the development of the specific cristae-like tubular morphology. No vesicle shape changes were observed when HCl was microinjected to GUV made only of PC/PE 66:34 mol/mol in buffer pH 8.

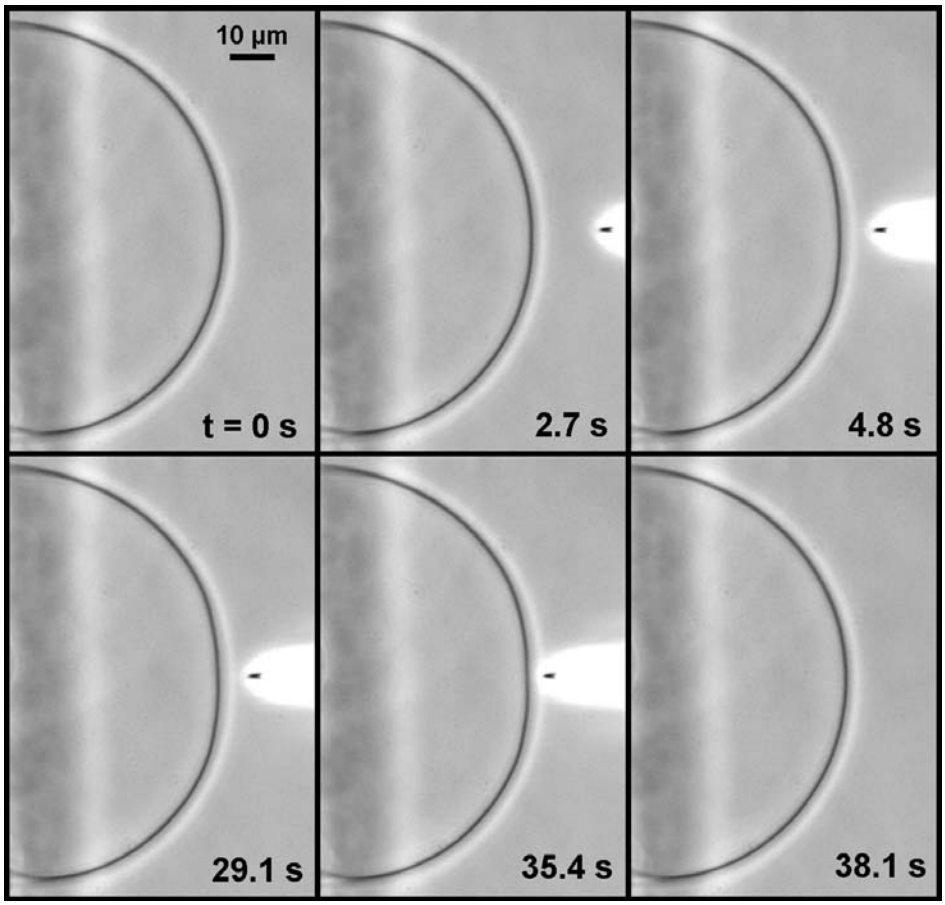

Fig. 5. Minimal membrane model exhibiting dynamic cristae-like morphology. GUV is made only of PC/CL 90:10 mol/mol in buffer pH 8. Without PE, local pH modulation induced cristae-like morphology similar to that observed with GUV made of PC/PE/CL 60:30:10 mol/mol, presented in Fig. 3.

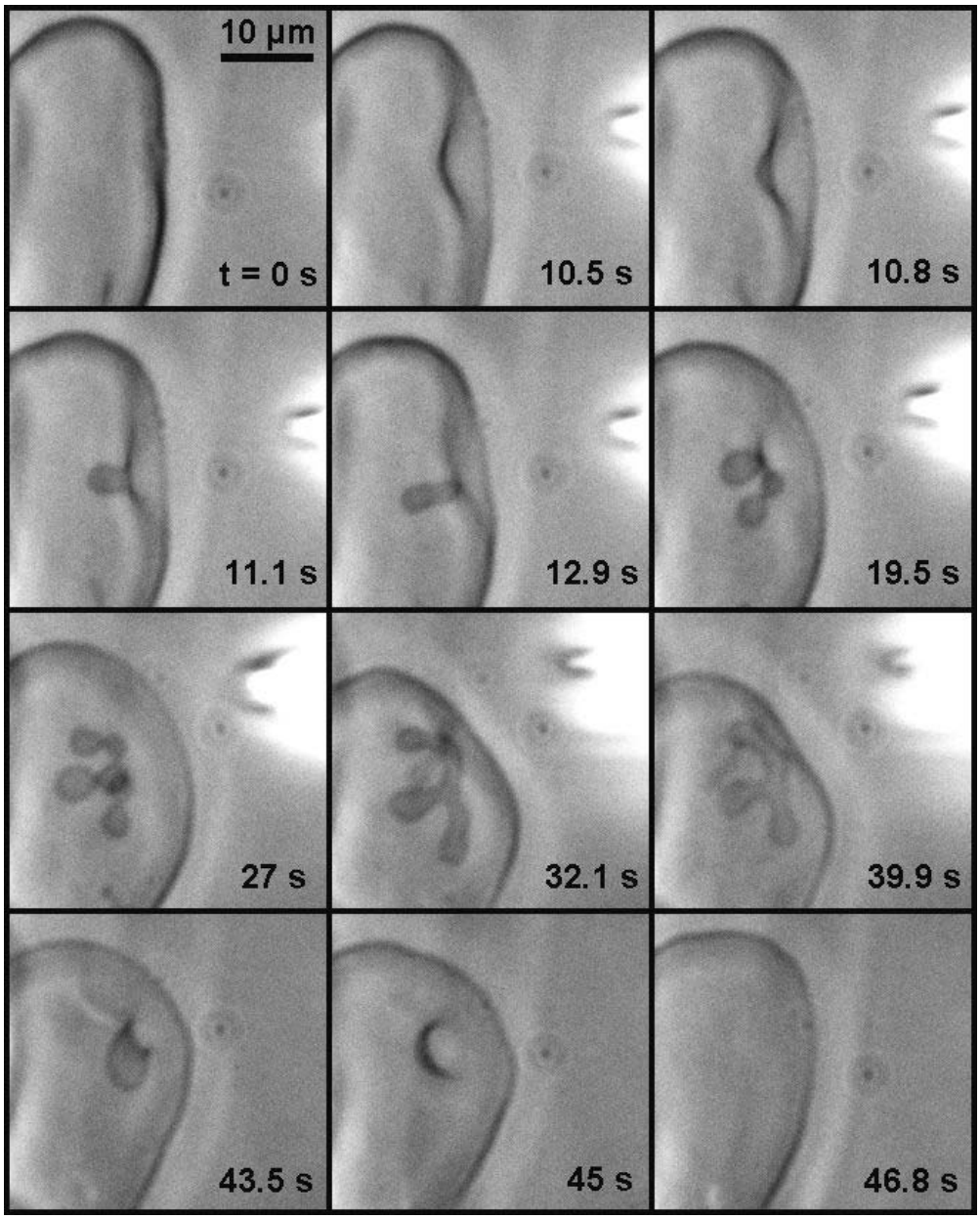

Fig. 6. Calculated Laurdan GP at pH 8 and pH 4 for different lipid mixtures. LUV are made of different lipid compositions with a Laurdan: lipid ratio of 1/200. PC; PC/CL 90:10 mol/mol; PC/PE 66:34 mol/mol; PC/PE/CL 60:30:10 mol/mol. All measurements were carried out at a lipid concentration of 0.2 mM and were recorded at 25°C. (grey) pH 8; (white) pH 4.

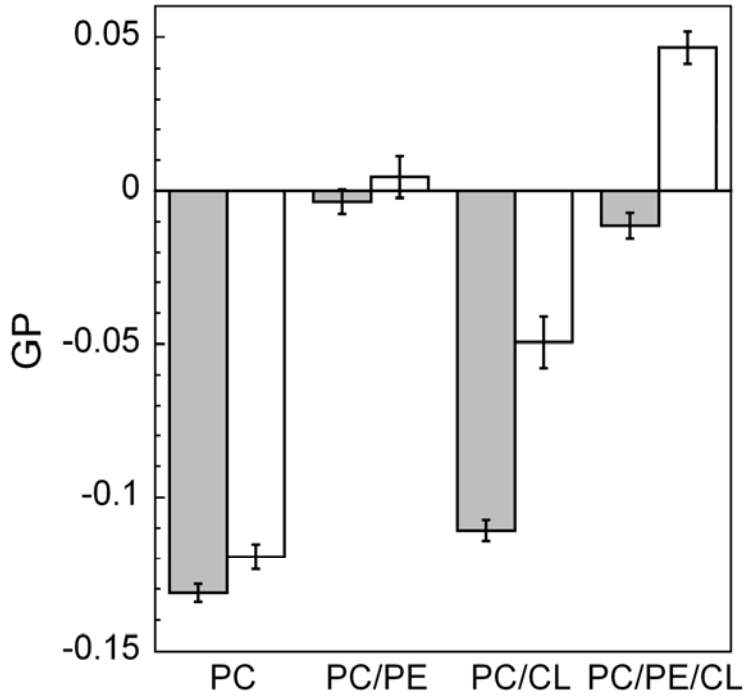

Fig. 7. Qualitative description of the dynamics of the shape instability. The lipids are drawn together with a constitutive-sphere indicating what their ideal, equilibrium density would be (see the text for more details). **(a)** Before the chemical modification. **(b)** Just after the chemical modification: the lipids of the outer-monolayer are effectively dilated (red or dark grey constitutive-spheres no longer in contact) but have not time to move yet. **(c)** First stage of the instability (lasting less than a μs): the lipids slide cooperatively with zero relative inter-monolayer velocity; this relaxes a fair amount of the dilation energy stored. **(d)** Curvature instability: the membrane bends in order to set the preferred density in both monolayers (green or light grey constitutive-spheres, in contact). For the lengths-scales involved, this bending mode is much faster than the relaxation involving inter-monolayer friction. The curvature instability is at the origin of the wiggling growth of the tubules from their base.

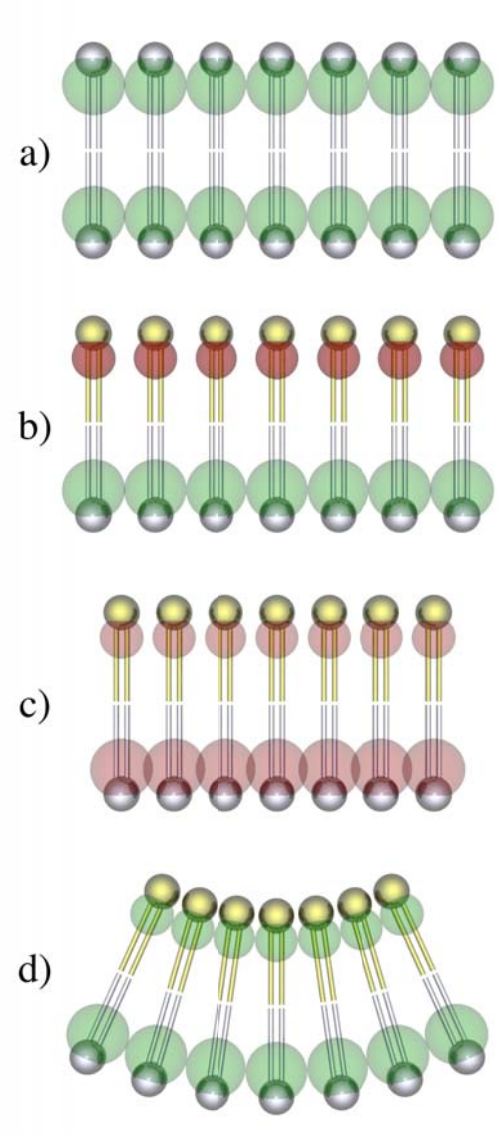

Table Legends

Table 1: Effect of pH on the ζ-potential of LUV made of different lipid mixtures

	ζ (mV)	
	pH 4	**pH 8**
PC	0.3	-7
PC/PE (66/34)	-4	-17
PC/PE/CL (60/30/10)	-46.4	-56
PC/CL (90/10)	-45	-56.9